Ab Initio Study of the Geometries and Vibrational Properties of the Low-Lying Electronic States of Neutral and Anionic M_3 (M = P, As, Sb, and Bi): The Photoelectron Spectroscopy of the Anions

Heechol Choi, Chungmin Park, and Kyoung K. Baeck*

Department of Chemistry, Kangnung National University, Kangnung, 210-702 Korea

Received: February 1, 2002

The geometries and vibrational properties of the low-lying electronic states of neutral and anionic of M_3 (M = P, As, Sb, and Bi) are studied using the coupled-cluster singles, doubles, and noniterative triples (CCSD(T)) method as well as the density functional theory (B3LYP-DFT) method. For P_3^-, the $^1\Sigma_g^+$ and $X^3A_1'(D_{3h})$ states are almost degenerate. The $X^3A_1'(D_{3h})$ state, however, turns out to be the lowest state for As_3^-, Sb_3^-, and Bi_3^-, and the adiabatic excitation energies of the $^1\Sigma_g^+$ state are 0.6, 0.9, and 1.0 eV, respectively. In the anionic trimers of all four elements, another singlet state, $^1A_1(C_{2v})$, is located about 0.3−0.4 eV above $X^3A_1'(D_{3h})$; the energy gap between these states is compared to the splittings between the first two peaks in the photoelectron spectra of these anions. For all of the neutral trimers, the adiabatic and vertical energetic splittings between the Jahn−Teller components of the X^2E'' and $^4E'$ states are calculated to be only 0.04−0.08 eV. Another quartet state, $^4A_2''$, is 0.4 eV higher, almost equal, 0.2 eV lower, and 0.3 eV lower in energy than the $^4E'$ state in P_3, As_3, Sb_3, and Bi_3, respectively. All of the features of the main peaks in the photoelectron spectra of the anions observed to date are explained by using calculated geometries, vibrational frequencies, and excitation energies. In addition, a number of peaks are predicted that have not yet been observed experimentally.

1. Introduction

The geometrical structure and spectroscopic properties of small metal clusters have attracted considerable interest over a long period. In addition to the numerous studies of the clusters of transition metal elements, clusters of group V elements (N, P, As, Sb, and Bi) have attracted special interest because of the ample variation in their properties on going from the light to the heavy members. Because the trimer of this series is the simplest possible cluster, a better understanding of its properties is indispensable to understanding the other clusters of group V elements.

Theoretical predictions of the differences between trimers of N and P were put forward quite some time ago[1−4] and are now well recognized. The theoretical work by Balasubramanian et al.[5] on the neutral and positive trimers of P, As, Sb, and Bi provided predictions for the properties of these trumers and has proved a useful guide in understanding experimental observations.

The advent of negative ion photoelectron spectroscopy and its application to the small clusters of group V elements produced experimental observations for Bi_n^- and Sb_n^- (n = 2−4) by Polak et al.,[6,7] for P_n^- (n = 1−9) by Jones et al.,[8] for Bi_n^- and Sb_n^- (n = 2−9) by Gausa et al.,[9] and for As_n^- (n = 1−5) by Lippa et al.[10] These experimental results were interpreted either by reference to earlier theoretical results[5] or through calculations that accompanied the experiments.[8,9] This body of work stimulated several theoretical studies.[11−14]

The elaborate experimental and theoretical studies carried out on the group V clusters have elucidated various aspects of their geometrical and spectroscopic properties. However, several aspects of the trimer are yet to be fully understood.

One of the most prominent features in the photoelectron spectra of P_3^-, As_3^-, Sb_3^-, and Bi_3^- is the relationship between the first two peaks.[6−10] Regardless of the element, the first peak is always slightly larger than the second. The splitting between the two peaks is also comparable for the different trimers: 0.28 eV in P_3^-, 0.36 eV in As_3^-, 0.14−0.16 eV in Sb_3^-, and 0.25−0.27 eV in Bi_3^-. The splitting in the photoelectron spectra of Sb_3^- and Bi_3^- was interpreted to arise from a combination of the Jahn−Teller effect and spin−orbit coupling. The splitting magnitudes are consistent with this hypothesis, although the splitting of 0.36 eV in the spectrum of As_3^- is rather large to be caused solely by the Jahn−Teller effect and the spin−orbit effect. Meanwhile, Jones et al.[8] suggested that the 0.28 eV splitting in the spectrum of P_3^- results from two distinct electron detachment processes from different anionic states. To the best of our knowledge, the origin of the splitting between the first two peaks in the photoelectron spectra of group V trimers is yet to be accounted for.

Another unresolved issue is the discrepancy in the literature regarding the position of the third peak in the photoelectron spectrum of Sb_3^-. In the spectrum obtained by Polak et al., the third peak appears as a weak peak at 3.312 eV electron binding energy (BE).[7] In contrast, Gausa et al.[9] detected no signal at around 3.3 eV but a strong peak at 3.65 eV BE. The discrepancy in the position of the third peak is unacceptable given that the BEs of the other main peaks from the two studies are within ±0.04 eV. The fact that the 3.65 eV BE is higher than the photon energy used by Polak et al. may account for the discrepancy; however, this discrepancy has yet to be discussed in detail.

* To whom correspondence should be addressed. E-mail: baeck@knusun.kangnung.ac.kr.

10.1021/jp020325x CCC: $22.00
Published on Web 04/25/2002

Problems are also evident in the existing data for the trimer systems of phosphorus. The electronic state producing the vibrational features in the spectrum of P_3^- [8] has not been completely resolved and remains a controversial subject. In addition, the observation more than a decade ago of a broad band system over the interval 480 ± 20 cm^{-1} in a vibronic absorption spectrum of P_3[16] has yet to receive proper theoretical support or interpretation.

We believe that the main reason for the problems outlined above is the lack of reliable theoretical calculations for the low-lying electronic states of the anionic trimers. The energetic separations among the $^3A_2'(D_{3h})$, $^1\Sigma_g^+$ $(D_{\infty h})$, and $^1A_1(C_{2v})$ states of P_3^- have been previously reported,[8] but little comparable work has been reported for As_3^-, Sb_3^-, or Bi_3^-. Most previous theoretical calculations have been limited to just the lowest electron binding energy and have paid little attention to other low-lying electronic states. In addition, reliable information about the geometries and vibrational properties of these systems is quite limited. More detailed and reliable information is an indispensable requirement for future experimental studies.

The first objective of the present work is to provide accurate data for the bond lengths, angles, and vibrational frequencies of the low-lying electronic states of the anionic and neutral trimers of phosphorus (P), arsenic (As), antimony (Sb), and bismuth (Bi). The second objective is to interpret all of the features in the previously obtained photoelectron spectra of the anionic trimers. We will also consider additional peaks, which were not observed in previous experiments because of their large electron binding energy.

2. Details of the Computations

The coupled-cluster singles, doubles, and noniterative triples (CCSD(T)) method[17,18] was the main computational tool used in the present study. The calculations using the CCSD(T) method were complemented by calculations using the gradient-corrected hybrid density functional theory (DFT) method. The CCSD(T) calculations were carried using the Aces-2 ab initio package,[19] whereas the DFT calculations were performed out using the B3LYP functional[20,21] method implemented in the Gaussian 98 suite of programs.[22] The G2 theory[23] of compound methods, implemented in Gaussian 98, was also applied for the near-degenerate states of P_3^- and some of the adiabatic electron binding energies.

The CCSD(T) method is one of the most accurate single-reference methods for electron correlation. On the other hand, the B3LYP functional is one of the most efficient and widely used DFT methods and produces reasonable results even for the electronic states with noticeable multireference character. We expect that the CCSD(T) and B3LYP-DFT methods provide a reliable and complementary pair for the purposes of the present predictive theoretical study.

Several basis sets were employed in this work. The P trimer was calculated using the aug-cc-pVTZ[24] all-electron basis sets, and the trimer systems of Sb and Bi were modeled using effective core potential (ECP) basis sets. The As systems, however, were calculated using both all-electron and ECP basis sets.

To obtain accurate and reliable results for the As trimers, a series of basis sets was used to try to come close to the near basis set limit. The B3LYP-DFT calculations were performed using the 6-31G(d), 6-311+G(d), and 6-311++G(3df) basis sets,[25,26] whereas the CCSD(T) calculations were carried out using the PVDZ+f, PVDZ+spdf, and 6-311++G(3df) basis sets. The PVDZ+f basis set was constructed from Ahlrich's PVDZ basis[27] by adding an f function ($\zeta_f = 0.372$) of Binning and Curtiss' VTZP set.[28] The PVDZ+spdf basis set was constructed by adding diffuse s, p, and d functions ($\zeta_s = \zeta_p = 0.034$, $\zeta_d = 0.0888$) to the PVDZ+f set.

To reduce the computational demands without deteriorating the reliability of the final results, the molecular orbitals (MO) corresponding to the 28 core electrons of each As atom were dropped in the post Hartree−Fock (HF) calculations. This approach will be referred to as the drop-MO method. The theoretical considerations and implementation of the analytic gradient of the CCSD(T) method[29] and its extension for use in the dropped MO space are described in detail elsewhere[30,31] and have been applied to the photoelectron spectroscopy of Al_3^- [32] and Ag_3^-.[33]

Another objective motivating the execution of intensive calculations on As trimer systems was to determine the proper size and quality of the ECP basis that should be used in calculations of clusters with heavier elements or a larger number of atoms of group V. To achieve this objective, two types of relativistic effective core potential (RECP) and their valence basis sets were employed. The LanL2+df basis was constructed by adding a d- and f-type function to the LanL2/RECP basis of Hay and Wadt.[34] The LanL2+dfspd basis was constructed by addition of diffuse s-, p-, and d-type functions to the LanL2+df basis. The same procedure was used to construct the SBKJ+df and SBKJ+dfspd basis sets based on the Stevenson's RECP and valence basis.[35] The exponents of the first d-type function and the s-, p-, and f-type functions were obtained using the procedure recently formulated by Gonzalea et al.[36] The exponent of the second diffuse d-type function was determined simply by multiplying the exponent of the first d-type function by 0.2. The exponents of these augmenting functions for As are 0.4420 (d), 0.7780 (f), 0.0690 (s), and 0.0212 (p) for the LanL2+ bases and 0.4980 (d), 0.5080 (f), 0.0226 (s), and 0.0226 (p) for the SBKJ+ bases.

Cartesian 6d and 10f basis functions were used for the 6-31G(d), 6-311+G(d), and 6-311++G(3df) bases, whereas the spherical 5d and 7f basis functions were employed for all other bases.

Only the RECP basis sets were employed in the calculations for the Sb and Bi trimer systems because of the lack of all-electron basis sets and to include relativistic effects. The exponents of the augmenting functions for the LanL2+ and SBKJ+ bases of Sb were the same as those generated by Gonzalea et al.[36] The exponents for the bases of Bi were generated by the procedure reported by Gonzalea et al.; the values are 0.1560 (d), 0.1090 (f), 0.0662 (s), and 0.0156 (p) for the LanL2+ basis and 0.1840 (d), 0.1190 (f), 0.0150 (s), and 0.0150 (p) for the SBKJ+dfspd basis.

3. Results and Discussion

Experimental studies have revealed several vibrational frequencies of P trimers, whereas no such information has been determined for other group V trimers. In section 3.1, we evaluate the reliability and accuracy of the theoretical methods used in the present work by comparing our calculated values with those from previous theoretical and experimental studies of P trimers.[8] In addition, we analyze the photoelectron spectrum of P_3^-.

We studied the trimer systems of As using both the all-electron and ECP basis sets. Special attention was given to these calculations because no previous report gives reliable information on the electronic states of As_3^-. The geometries and vibrational frequencies of the low-lying electronic states of anionic and neutral As trimer systems are discussed in section 3.2.

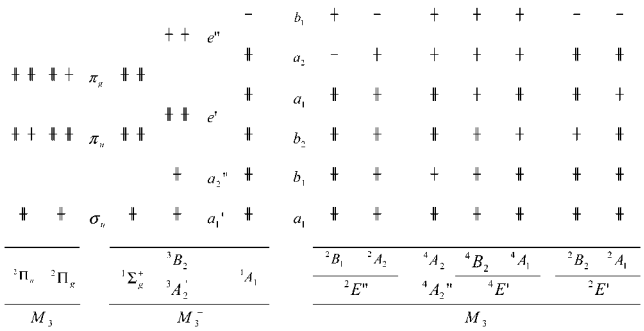

Figure 1. Nonrelativistic electronic configurations of the low-lying states of neutral and negative trimers of group V elements.

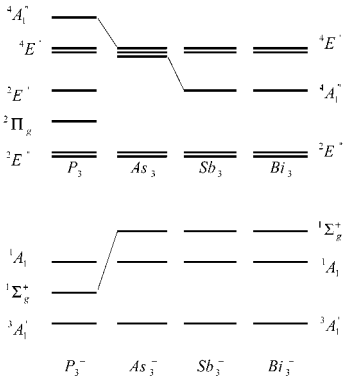

Figure 2. Energy levels of M_3^- (lower) and M_3 (upper).

Section 3.3 presents the results for trimer systems of Sb and Bi, obtained from calculations using only ECP basis sets. The bond lengths, bond angles, vibrational frequencies, and energetic separations are compared with the corresponding values for the trimer systems of P and As.

Finally, in section 3.4, the photoelectron spectra of As_3^-, Sb_3^-, and Bi_3^- are analyzed by using the calculation results presented in preceding sections. The similarities and differences of the P, As, Sb, and Bi trimer systems are discussed.

To facilitate the understanding of the discussion presented below, schematic diagrams of the nonrelativistic electronic configurations of the low-lying electronic states and the relationships among these states are given in Figures 1 and 2, respectively. The correlation among the electronic states in different geometrical symmetries is discussed in greater detail by Burdett et al.[3] The convention of the symmetry representation of C_{2v} is taken to be that E of D_{3h} corresponds to $A_2 \oplus B_1$ of C_{2v}.

3.1. Structure and Photoelectron Spectroscopy of the Phosphorus Trimer: P_3^- and P_3. Table 1 lists the bond length, bond angle, adiabatic energy difference, and vibrational frequency of low-lying electronic states of P_3^- and P_3. The near degeneracy of the low-lying states of P_3^-, which was first discussed a decade ago by Hamilton and Schaefer,[4] is shown in the upper part of Table 1. The energy of the $^1\Sigma_g^+$ state as calculated by the CCSD(T) and B3LYP methods is 3.6 and 4.0 kcal/mol higher than that of the $^3B_2(^3A_2')$ state, respectively. The energy difference calculated by CCSD(T) increases to 4.1 kcal/mol by full inclusion of the triple excitation in the CCSDT method[37,38] but decreases to 2.1 kcal/mol on inclusion of the core electrons into the electron correlation within the CCSD(T) method. Therefore, the CCSDT value including the core−electron correlation is expected to be about 2.6 kcal/mol. Hamilton and Schaefer reported values of 2.1 and 0.9 kcal/mol obtained from calculations using the MR−CISD/DZP//CASSCF/DZP method and the MR−CISD/DZP//CASSCF/DZP plus quadruple corrections, respectively.[4] To obtain another viewpoint, we applied the G2 theory method,[23] and the method locates the $^1\Sigma_g^+$ state 0.8 kcal/mol *below* the $^3B_2(^3A_2')$ state. Thus, the values we obtained using the CCSD(T) and B3LYP methods support and augment the result of Hamilton and Schaefer, whereas the G2 method gave the opposite result. Therefore, the relative energy between $^3B_2(^3A_2')$ and $^1\Sigma_g^+$ remains one of the most challenging problems confronting theoretical and experimental studies of the P_3^- system.

Another low-lying electronic state of the P_3^- system is the $^1A_1(C_{2v})$ state of the bent structure. The $^1A_1$ state is calculated to be 7.3 and 10.1 kcal/mol higher in energy than the $^3B_2(^3A_2')$ state by the CCSD(T) and B3LYP methods, respectively. These results are comparable to the values of 6.2, 6.4, and 5.5 kcal/mol reported by Jones et al.,[8] Burdett et al.,[3] and Hamilton et al.,[4] respectively. All of the calculations, past and present, locate the $^1A_1$ state 4−6 kcal/mol above the $^1\Sigma_g^+$ state. Burdett et al.[3] explained the reason of the barrier between the bent and linear singlet states and calculated the barrier between $^1A_1$ and $^1\Sigma_g^+$ as 25 kcal/mol using the MBPT[3] method.[3] Our calculations using the B3LYP/aug-cc-pVTZ method predict the barrier to be 42 kcal/mol.

An intense infrared band at 815 cm^{-1} was observed in an experimental study of P_5^-.[35] Hamilton and Schaefer[4] showed that the linear singlet state of P_3^- ($^1\Sigma_g^+$) is responsible for this IR peak, although their calculations using the SCF/DZP method gave a frequency of 886 cm^{-1}. In the present calculations, the $\omega(\sigma_u^-)$ of the $^1\Sigma_g^+$ state was found to be 802 and 800 cm^{-1} using the CCSD(T) and B3LYP methods, respectively. Our results therefore confirm Hamilton and Schaefer's identification of the IR peak.

Jones et al. observed a vibrational structure in the first peak of the P_3^- photoelectron spectrum and suggested that this structure corresponds to either one vibration of 390 ± 50 cm^{-1} or two vibrations of 340 ± 40 and 435 ± 40 cm^{-1}. Jones et al. assigned the vibrational structure to two vibrations of the $^1A_1(C_{2v})$ state, but the agreement with their calculated frequencies was not satisfactory as they mentioned.[8]

According to our B3LYP calculations, the $\omega(b_2)$ of $^1A_1$ is very close to 435 ± 40 cm^{-1}, but the $\omega(a_1)$ is a little away from the experimentally suggested range, 340 ± 40 cm^{-1}. Meanwhile, the $\omega(e')$ of $^3B_2$ state is found to be 412−418 cm^{-1}, which is close to the experiment-based suggestion of a single vibration at 390 ± 50 cm^{-1}. The uncertainties in both the experimental and theoretical values make it difficult to reach a conclusion. However, the bond lengths and angles calculated in the present study show that the geometrical change associated with the $P_3(^2B_1,^2A_2) \leftarrow P_3^-(^3B_2)$ transition is smaller than that of the $P_3(^2B_1,^2A_2) \leftarrow P_3^-(^1A_1)$ transition. This observation supports the hypothesis that the $^3B_2$ state is the source of a single vibration of 390 ± 50 cm^{-1}. The vertical electron detachment energy, which will be discussed below, also supports this interpretation.

The geometries and vibrational frequencies of the three lowest electronic states of P_3 were also investigated and are given in the lower part of Table 1. The geometrical and energetic relationships between the E'' state and its Jahn−Teller components (the A_2 and B_1 states) are described by Balasubramanian et al.[5] Their MRCI/RECP calculation locates the $^2A_2$ state 5.1 kcal/mol below the $^2B_1$ state. Similarly, our calculations using the B3LYP method locate the $^2A_2$ state 0.4 kcal/mol below the $^2B_1$ state. The order of states, however, is reversed in the result from the CCSD(T) method, which gives a 0.8 kcal/mol energy

TABLE 1: Bond Length (R_e in Å), Angle ($\angle$ in Degrees), Adiabatic Energy Difference (ΔE in kcal/mol), and Harmonic Frequency (ω in cm^{-1}) of Low-lying Electronic States of P_3^- and P_3 by Using the aug-cc-pVTZ Basis

	state	method	R_e	$\angle$	ΔE	ω (calcd)	ω (expt)
P_3^-	$^3B_2$	CCSD(T)	2.1827	60.0	0.0[a]	418(e'), 570(a_1')	390 ± 50[g]
		B3LYP	2.1811		0.0[a]	412, 562	
		others[c]	2.174		0.0	457,641	
		others[d]	2.159		0.0	427,572	
	$^1\Sigma_g^+$	CCSD(T)	1.9743	180.0	3.6	162(π_u), 474(σ_g^+), 802(σ_u^-)	815[h]
		B3LYP	1.9623		4.0	171, 482, 800	
		others[c]	1.943		0.9	188,552,886	
		others[d]	1.970		−1.4	176,482,809	
	$^1A_1$	CCSD(T)	2.0872	73.1	7.3	280(a_1),605(a_1)	340/435 ± 40[g]
		B3LYP	2.0760	73.2	10.1	289,614,433(b_2)	
		others[c]	2.065	73.0	6.4	337,686,158	
		others[d]			4.8	313,607,449	
	$^1A_1$(TS)[e]	B3LYP	2.0698	115.0	42.1		
P_3	$^2B_1$	CCSD(T)	2.2092	55.3	0.0[b]	462(a_1), 635(a_1)	460 ± 65[g],645 ± 60[g]
		B3LYP	2.2042	55.0	0.0[b]	462, 650	
		others[f]	2.21	55.0	0.0		
	$^2A_2$	CCSD(T)	2.0942	65.5	0.8	399(a_1), 631(a_1)	
		B3LYP	2.0892	65.6	−0.4	399, 625	
		others[d]				409,623,334(b_2)	
		others[f]	2.10	66.7	−5.1		
	$^2\Pi_g$	CCSD(T)	1.9726	180.0	31.1	119(π_u), 483(σ_g^+), 629(σ_u^-)	480 ± 20[i]
		B3LYP	1.9638		47.4	116, 482,681	

[a] The total energies of $^3B_2$ state by the CCSD(T) method and the B3LYP method are −1022.772159 au and −1024.191166 au, respectively. [b] The total energies of $^2B_1$ state by the CCSD(T) method and the B3LYP method are −1022.711783 au and −1024.127496 au, respectively. [c] The R_e and ω in ref 4 are calculated by the CISD/TZ2P and SCF/DZP method, respectively. [d] The MD/DF result in ref 8. [e] The transition structure between the $^1\Sigma_g^+$ and the $^1A_1$ state. [f] The MRCI/RECP result in ref 5. [g] The vibrational features in the photoelectron spectrum of ref 8. [h] Reference 34. [i] Reference 16.

gap. The G2 method[23] also reverses the order of the states, locating the $^2A_2$ state 0.2 kcal/mol above the $^2B_1$ state. The adiabatic energy separation between the two states seems to be almost zero.

The vibrational frequencies of the $^2B_1$ state calculated in the present work (462 and 635−650 cm^{-1}) are in quite good agreement with the experimentally vibrations of 460 ± 65 and 645 ± 60 cm^{-1}. The frequency of the symmetric stretch mode is almost the same in $^2B_1$ and $^2A_2$, whereas the bending frequency of the $^2B_1$ state is about 60 cm^{-1} larger than that of the $^2A_2$ state.

Balasubramanian et al. have shown that the neutral trimer of P can have a linear structure as a local energetic minimum but other natural trimers of group V cannot. We also studied the geometry and vibrational properties of the $^2\Pi_g$ state of P_3. About a decade ago, Andrew and Mielke observed a broad band system with the interval of 480 ± 20 cm^{-1} in the vibronic absorption spectrum of P_3.[16] They attributed this band to a fundamental, and presumably symmetric, stretching mode in an excited state of P_3; however, to date there has been no theoretical or experimental confirmation of this conjecture. In the present work, the $\omega(\sigma_g^+)$ of $^2\Pi_g$ was calculated to be 482−483 cm^{-1}, which is in good agreement with the experimental value.

The data obtained from the present calculations are sufficiently accurate to explain all of the features in the photoelectron spectrum of P_3^-.[8] We calculated the electronic energy of the low-lying electronic states of P_3 ($^4B_2$, $^4A_1$, $^4A_2$, $^2B_2$, $^2A_1$, and $^2\Pi_u$) by using their distinctive electron configurations in the CCSD(T) method. The adiabatic and vertical electron binding energies (ABE and VBE) to the states of P_3 were then computed, and the results were compared with previous theoretical and experimental values (see Table 2).

First, the vertical and adiabatic Jahn−Teller splittings of the E'' state were calculated to be less than 0.04 eV. In view of the fact that the splitting between the first two peaks in the spectrum of P_3^- is 0.28 eV, it is unlikely that the Jahn−Teller effect is the source of the splitting. The spin−orbit splittings in the ^2D and ^2P states of atomic phosphorus are only 14.7 and 25.7 cm^{-1}, which suggests that spin−orbit coupling can also be ruled out as the source of the splitting in the spectrum.

TABLE 2: Adiabatic and Vertical Electron Binding Energy (ABE and VBE in eV) of Electron Detachment Processes of P_3^-

transition	method	ABE	VBE	expt[a]
$P_3(^2A_2) \leftarrow P_3^-(^1A_1)$	CCSD(T)	1.35	1.56	1.68
	B3LYP	1.28	1.48	
	MD/DF[c]		1.73	
$P_3(^2B_1,^2A_2) \leftarrow P_3^-(^3B_2)$	CCSD(T)	1.64,1.68	1.81,1.85	1.96
	B3LYP	1.73	1.89	
	MD/DF[c]		1.88	
$P_3(^2\Pi_g) \leftarrow P_3^-(^1\Sigma_g^+)$	CCSD(T)	2.84	2.84	2.89
	B3LYP	2.75	3.13	
	MD/DF[c]		3.00	
$P_3(^2B_2,^2A_1) \leftarrow P_3^-(^1A_1)$	CCSD(T)		3.52,3.53	weak signals[b]
	MD/DF[c]		3.70	
$P_3(^4B_2,^4A_1) \leftarrow P_3^-(^3B_2)$	CCSD(T)		3.94,3.95	3.91
	B3LYP		3.97	
	MD/DF[c]		4.08	
$P_3(^4A_2) \leftarrow P_3^-(^3B_2)$	CCSD(T)		4.32	4.32
$P_3(^2B_2,^2A_1) \leftarrow P_3^-(^3B_2)$	CCSD(T)		4.96,5.08	

[a] The peak maximum of the photoelectron spectroscopy in ref 8. [b] Our interpretation; see the text for detail. [c] From ref 8.

Jones et al. suggested that the first two peaks can be attributed to two processes from two different anionic systems, with the first peak corresponding to $P_3(^2A_2) \leftarrow P_3^-(^1A_1)$ and the second peak corresponding to $P_3(^2B_1,^2A_2) \leftarrow P_3^-(^3B_2)$. In the present work, the VBE of $(^2A_2) \leftarrow P_3^-(^1A_1)$ was calculated to be 1.56 (1.48) eV using the CCSD(T)(B3LYP) method. This interpretation also implies that the vibrational structure in the first peak corresponds to a single vibration of 390 ± 50 cm^{-1}, as discussed above. The VBE of the $P_3(^2B_1$ or $^2A_2) \leftarrow P_3^-(^3B_2)$ transition, on the other hand, turns out to be 1.81−1.85 and 1.89 eV by the CCSD(T) and the B3LYP method, respectively.

TABLE 3: Total Energy (E_{tot} in Hartree), Bond Length (R_e in Å), and Angle ($\angle$ in Degrees) of the Low-Lying Electronic States of As_3^-[a]

	$^3B_2(C_{2v}) = {}^3A_1'(D_{3h})$		$^1A_1(C_{2v})$			$^1\Sigma_g^+(D_{\infty h})$	
method	E_{tot}	R_e	T_e	R_e	$\angle$	T_e	R_e
CCSD(T)/PVDZ+f	−6702.240462	2.408	0.44	2.310	72.3	0.65	2.187
CCSD(T)/PVDZ+spdf	−6702.272112	2.420	0.37	2.322	71.9	0.56	2.201
CCSD(T)/6-311++G(3df)	−6702.575702	2.417	0.37	2.319	71.8	0.60	2.198
G2			0.17			0.41	
B3LYP/6-31G(d)	−6701.346795	2.404	0.52	2.297	71.8	0.66	2.167
B3LYP/6-311+G(d)	−6707.730287	2.425	0.43	2.316	72.1	0.58	2.191
B3LYP/6-311++G(3df)	−6707.737854	2.414	0.44	2.305	72.0	0.57	2.183
CCSD(T)/LANL2+df	−18.311608	2.390	0.44	2.294	76.6	0.48	2.173
CCSD(T)/LANL2+dfspd	−18.369505	2.406	0.34	2.307	72.7	0.42	2.189
CCSD(T)/SBKJ+df	−18.610875	2.380	0.42	2.285	72.5	0.64	2.170
CCSD(T)/SBKJ+dfspd	−18.666121	2.400	0.35	2.301	72.5	0.50	2.183
B3LYP/LANL2+df	−18.454981	2.434	0.56	2.322	72.8	0.46	2.186
B3LYP/LANL2+dfspd	−18.475559	2.420	0.49	2.311	72.2	0.54	2.186
B3LYP/SBKJ+df	−18.754819	2.421	0.52	2.310	72.4	0.59	2.182
B3LYP/SBKJ+dfspd	−18.762095	2.420	0.48	2.304	72.4	0.59	2.183

[a] Adiabatic excitation energy (T_e in eV) is defined with respect to $^3B_2$ state.

When the VBEs obtained using the CCSD(T) method are compared with the two peak maxima of the spectrum (1.68 and 1.96 eV), the CCSD(T) method is found to consistently underestimate the VBE by about 0.1 eV. We therefore expect that the VBE and ABE calculated using the CCSD(T)/aug-cc-pVTZ method should be corrected by about +0.1 eV. We have used a correction of a similar magnitude (+0.11 eV) in a previous application of the drop-MO CCSD(T) method to the photoelectron spectra of Al_3^-.[32]

The location of the third peak of the spectrum, 2.89 eV, matches very well with the calculated VBE of the $P_3(^2\Pi_g) \leftarrow P_3^-(^1\Sigma_g^+)$ process. The bond length change in this transition is less than 0.002 Å, as calculated from the values in Table 1. The vibrational frequencies of the $^1\Sigma_g^+$ state are also very similar to the corresponding values of the $^2\Pi_g$ state. As mentioned by Jones et al., these facts agree with the vertical transition nature indicated by the narrow and symmetric shape of the third peak.

Our calculations predict that another peak, corresponding to the second electron detachment process from the $^1A_1$ state, should appear in the photoelectron spectrum at 3.3 (B3LYP) or 3.5 eV (CCSD(T)) BE. Jones et al. calculated that the peak should appear at 3.70 eV. However, the photoelectron spectrum of P_3^- of Jones et al. shows a number of undefined weak signals corresponding to a BE of 3.2−3.5 eV, which they did not explicitly point out. We suggest that these weak signals are the result of the electron detachment process of $P_3(^2B_2$ or $^2A_1) \leftarrow P_3^-(^1A_1)$.

No explanation has been previously given for the fourth and fifth main peaks. According to our calculations, the fourth peak at 3.91 eV BE corresponds to the $P_3(^4B_2,^4A_1) \leftarrow P_3^-(^3B_2)$ transition and the fifth peak at 4.32 eV BE results from the $P_3(^4A_2) \leftarrow P_3^-(^3B_2)$ transition. The results of present work also suggest the presence of an additional peak at about 5.0 eV BE, which has not been observed experimentally.

3.2. Structure of the Arsenic Trimer: As_3, As_3^-, and As_3^+. The bond lengths (R_e in Å), angles ($\angle$ in degrees), and adiabatic excitation energies (T_e in eV) of the low-lying electronic states of As_3^- are given in Table 3, and their harmonic frequencies are given in Table 4. The present results are not compared with any previous results because of the lack of relevant theoretical or experimental data. The T_e of $^1A_1$ and $^1\Sigma_g^+$ states of As_3^- is defined with respect to the $^3B_2$ state. The results from the calculations using all-electron basis sets, which were undertaken to obtain highly accurate theoretical results, are given in the upper part of Tables 3 and 4 and will be discussed first.

TABLE 4: Vibrational Frequencies (ω in cm^{-1}) of the Low-Lying Electronic States of As_3^-[a]

	$^3B_2$		$^1A_1(C_{2v})$			$^1\Sigma_g^+(D_{\infty h})$		
	e'	a_1'	$a_{1,bend}$	b_2	$a_{1,str}$	π_u	σ_g	σ_u
CCSD(T)/PVDZ+spdf	238	330	163		343	79	267	442
CCSD(T)/6-311++G(3df)	240	330	164		343	76	261	439
B3LYP/6-311+G(d)	230	322	165	242	344	21	262	432
B3LYP/6-311++G(3df)	232	324	168	241	346	81	264	435
	(0.3)		(0.1)	(43.8)	(0.1)	(0.6)		(86.8)
CCSD(T)/LANL2+df	241	332	123		340	63	268	462
CCSD(T)/LANL2+dfspd	227	320	156		336	76	260	443
CCSD(T)/SBKJ+df	242	334	160	259	347	−45	264	449
CCSD(T)/SBKJ+dfspd	233	322	155		337	61	258	430
B3LYP/LANL2+df	231	312	163	246	334	83	264	444
B3LYP/LANL2+dfspd	231	318	164	240	341	85	264	435
B3LYP/SBKJ+df	228	312	166	237	335	69	258	425
B3LYP/SBKJ+dfspd	228	315	164	234	339	80	260	426
	(0.3)		(0.1)	(43.7)	(0.1)	(1.0)		(90.8)

[a] The infrared intensities (in km/mol) are given in parentheses.

The values of R_e, $\angle$, and T_e calculated using the CCSD(T) and B3LYP-DFT methods with all-electron basis sets showed convergent behavior within each calculation method. Comparing the results for the CCSD(T)/6-311++G(3df) and B3LYP/6-311++G(3df) methods, we see that the maximum differences in the values of R_e, $\angle$, T_e, and ω are 0.015 Å, 0.2°, 0.07 eV, and 8 cm^{-1}, respectively.

The values of T_e in Table 3 show that in As_3^- the two states ($^3B_2$ and $^1\Sigma_g^+$) are no longer nearly degenerate, in contrast to the near degeneracy of these states in P_3^-. Our calculations using the CCSD(T) and B3LYP methods predict that the $^1A_1$ and $^1\Sigma_g^+$ states lie approximately 0.4 and 0.6 eV higher in energy than the $^3B_2$ state, respectively. These energetic separations reduce to 0.17 and 0.41 eV when the calculation is performed using the G2 method.[23]

The bond lengths of the $^1\Sigma_g^+$, $^1A_1$, and $^3B_2$ states of As_3^- are 0.22−0.33 Å longer than the corresponding lengths in P_3^-, and the vibrational frequencies of As_3^- are smaller than those of P_3^-. According to the B3LYP/6-31+G(d) method, the transition state from $^1A_1$ to $^1\Sigma_g^+$ has $R_e = 2.283$ Å and $\angle = 114.4°$ and is located 29.9 kcal/mol above the $^1A_1$. These transition state characteristics are comparable to those of P_3^-.

The geometries and vibrational properties of five low-lying electronic states of As_3 are shown in Tables 5 and 6. The

TABLE 5: Results for the Low-Lying Doublet and Quartet State of As_3[a]

	$^2E''(D_{3h})$								$^4E'(D_{3h})$					
	$^2B_1(C_{2v})$			$^2A_2(C_{2v})$			$^4A_2''(D_{3h})$		$^4B_2(C_{2v})$			$^4A_1(C_{2v})$		
	ΔE	R_e	$\angle$	T_e	R_e	$\angle$	T_e	R_e	T_e	R_e	$\angle$	T_e	R_e	$\angle$
CCSD(T)/PVDZ+f	1.26	2.444	55.5	+0.04	2.326	65.1	1.92	2.515	1.95	2.365	66.3	1.97	2.489	55.8
CCSD(T)/PVDZ+spdf	1.73	2.450	55.5	+0.04	2.331	65.1	1.91	2.521	1.90	2.371	66.5	1.93	2.500	55.7
CCSD(T)/6-311++G(3df)	1.71	2.448	55.5	+0.04	2.328	65.1	1.91	2.519	1.90	2.370	66.5	1.93	2.499	55.6
B3LYP/6-31G(d)	1.42	2.431	55.2	−0.01	2.315	65.0	1.91	2.506	1.89	2.359	66.7	1.92	2.492	55.5
B3LYP/6-311+G(d)	1.81	2.450	55.2	−0.02	2.330	65.2	1.83	2.528	1.84	2.377	67.2	1.87	2.523	55.1
B3LYP/6-311++G(3df)	1.81	2.440	55.2	−0.02	2.321	65.2	1.85	2.518	1.83	2.366	67.2	1.86	2.508	55.3
CCSD(T)/LanL2+df	1.05	2.425	55.4	+0.04	2.306	65.2	1.95	2.501	2.00	2.339	66.7	2.04	2.467	55.7
CCSD(T)/LanL2+dfspd	1.55	2.439	55.3	+0.04	2.315	65.3	1.93	2.515	1.95	2.353	67.1	1.98	2.490	55.4
CCSD(T)/SBKJ+df	1.26	2.413	55.4	+0.03	2.295	65.1	1.93	2.486	1.99	2.333	66.7	2.02	2.463	55.5
CCSD(T)/SBKJ+dfspd	1.56	2.430	55.4	+0.04	2.308	65.2	1.92	2.506	1.95	2.350	67.0	1.98	2.487	55.4
B3LYP/LanL2+df	1.61	2.458	55.0	−0.03	2.337	65.2	1.72	2.543	1.80	2.379	67.7	1.84	2.525	55.2
B3LYP/LanL2+dfspd	1.82	2.447	55.1	−0.03	2.328	65.2	1.76	2.527	1.80	2.371	67.5	1.84	2.516	55.2
B3LYP/SBKJ+df	1.78	2.446	55.0	−0.03	2.326	65.2	1.52	2.527	1.78	2.372	67.6	1.81	2.521	55.0
B3LYP/SBKJ+dfspd	1.75	2.442	55.0	−0.03	2.321	65.3	1.73	2.522	1.79	2.368	67.6	1.82	2.517	55.0
others/MRCI[b]		2.48	55.0	−0.05	2.35	65.5	1.89	2.56	(2.19	2.46	60.0	2.19	2.46	60.0)[c]

[a] Energy Differences (ΔE in eV) of the $^2B_1$ is Defined Relative to the $^3B_2$ of As_3^-, Whereas T_e (in eV) is Calculated Relative to $^2B_1$ state. [b] Reference 5. [c] The result with fixed angle of 60.0°.

TABLE 6: Vibrational Frequencies of the Lowest Doublet and Quartet States of As_3[a]

	$^2E''(D_{3h})$						$^4E'(D_{3h})$			
	$^2B_1$		$^2A_2$		$^4A_2''(D_{3h})$		$^4B_2$		$^4A_1$	
	$(a_1)_{str}$	$(a_1)_{bend}$	$(a_1)_{str}$	$(a_1)_{bend}$	$\omega(a_1')$	$\omega(e')$	$(a_1)_{str}$	$(a_1)_{bend}$	$(a_1)_{str}$	$(a_1)_{bend}$
CCSD(T)/PVDZ+spdf	361	262	358	227	295	218	323	181	331	237
CCSD(T)/6-311++G(3df)	360	262	357	227	294	218	320	182	333	238
B3LYP/6-311+G(d)	365	259	353	224	290	214	316	172	326	227
B3LYP/6-311++G(3df)	367	260	354	226	291	215	318	176	328	229
	(0.1)	(0.1)	(0.0)	(0.1)		(0.8)	(0.4)	(0.3)	(0.3)	(1.9)
CCSD(T)/LanL2+dfspd	355	257	351	222	281	210	315	174	326	228
CCSD(T)/SBKJ+spddf	356	259	360	226	280	200	316	174	326	230
B3LYP/LanL2+dfspd	362	258	345	225	285	213	308	169	322	224
B3LYP/SBKJ+dfspd	361	256	343	223	285	212	306	169	319	222
	(0.1)	(0.0)	(0.0)	(0.1)		(0.8)	(0.3)	(0.3)	(0.4)	(1.9)

[a] All symbols have the same meaning as in Table 4.

adiabatic energy difference (ΔE) of the $^2B_1$ state of As_3 is calculated relative to the $^3B_2$ state of As_3^-. The T_e's of the other states in Table 5 are defined with respect to the $^2B_1$ state of As_3. As shown by Balasubramanian et al.,[5] the $^2\Pi_g$ state of As_3 is no longer a stationary point on the potential energy surface, and its geometry is therefore not calculated here.

The results presented in Table 5 indicate that the degenerate $^2E''(D_{3h})$ state is distorted and split into $^2B_1(C_{2v})$ and $^2A_2(C_{2v})$ states. Although the CCSD(T)/6-311++G(3df) method locates the $^2B_1$ state 0.04 eV below the $^2A_2$ state, the B3LYP/6-311++G(3df) method predicts the reverse order with an energy separation of 0.02 eV. The G2 theory method also locates $^2B_1$ below $^2A_2$, with an energy difference of 0.05 eV.

The degenerate $^4E'(D_{3h})$ state, which is located about 1.9 eV above the $^2E''$ state, also shows Jahn−Teller splitting into $^4B_2(C_{2v})$ and $^4A_1(C_{2v})$ states. The $^4B_2$ state is predicted to lie below the $^4A_1$ state by both the CCSD(T) and B3LYP methods. However, the energy separation between them is very small (0.03 eV).

Another quartet state, $^4A_2''(D_{3h})$, is calculated to be almost isoenergetic with the $^4E'$ state. This result stands in contrast to the case of P_3, for which the $^4A_2''$ state is located approximately 0.4 eV above the $^4E'$ state, as shown in Figure 2.

We now assess the reliability of the CCSD(T) and B3LYP methods with the RECP basis sets. To facilitate comparison, we collate the results obtained using the two methods with the RECP basis sets in the lower parts of Tables 3−6. If the results with RECP are compared within themselves, the difference between the LANL2+df result and the SBKJ+df result decreases on augmentation with diffuse s-, p-, and d-type functions. In addition, we tested other choices for the augmentations such as LanL2(or SBKJ)+d and LanL2(or SBKJ)+dfsp. It was found that the LanL2(or SBKJ)+df bases are the smallest bases that give reliable results. Although the geometries and vibrational frequencies obtained using the LanL2(SBKJ)+df basis are already good enough, the diffuse functions were added to ensure that the basis set limit had been reached, especially with regard to the electron binding energies and excitation energies. We regard the results obtained using the LanL2(or SBKJ)+dfspd basis to be very close to the basis-set limit within the method with RECP.

The results in Tables 3−6 calculated using the all-electron basis are well reproduced by using the RECP basis. The differences between the RECP-basis limit of the CCSD(T) (or B3LYP) method and the corresponding all-electron-basis limit are less than 0.02 Å and 0.7 degrees for R_e and $\angle$, respectively. The difference is smaller in the B3LYP method than in the CCSD(T) method.

The CCSD(T)/LanL2(SBKJ)+dfspd method slightly *overestimates* the value of T_e with respect to the CCSD(T)/6-311++G(3df) method, whereas the B3LYP/LanL2(SBKJ)+dfspd method *underestimates* the value with respect to the B3LYP/6-311++G(3df) method. As a result, the maximum differences between the limiting values of T_e obtained using the CCSD(T) and B3LYP methods with the RECP are about 0.13 eV, whereas the maximum difference is 0.07 eV with the 6-311++G(3df)

TABLE 7: Results for Sb_3^- and Bi_3^-[a]

	$^3B_2(D_{3h};M_3^-)$		$^1A_1(C_{2v})$			$^1\Sigma_g^+(D_{\infty h};M_3^-)$	
	E_{tot}	R_e	T_e	R_e	$\angle$	T_e	R_e
			Sb_3 Systems				
CCSD(T)/LanL2+dfspd	−16.252108	2.810	0.39	2.714	69.7	0.91	2.588
CCSD(T)/SBKJ+dfspd	−16.377046	2.785	0.39	2.690	69.8	0.91	2.565
B3LYP/LanL2+dfspd	−16.346253	2.808	0.50	2.698	70.1	0.90	2.568
B3LYP/SBKJ+dfspd	−16.475551	2.782	0.50	2.674	70.1	0.89	2.545
			Bi_3 Systems				
CCSD(T)/LanL2+dfspd	−16.354340	2.957	0.36	2.857	69.5	1.05	2.725
CCSD(T)/SBKJ+dfspd	−16.380587	2.965	0.36	2.866	69.5	1.03	2.736
B3LYP/LanL2+dfspd	−16.528413	2.918	0.47	2.805	69.9	1.04	2.677
B3LYP/SBKJ+dfspd	−16.550669	2.934	0.49	2.820	69.8	1.05	2.692

[a] All symbols have the same meaning as in Table 3.

TABLE 8: Results for Sb_3^- and Bi_3^-[a]

	$^3B_2(D_{3h};M_3^-)$		$^1A_1(C_{2v};M_3^-)$			$^1\Sigma_g^+(D_{\infty h};M_3^-)$		
	e'	a_1'	$a_{1,bend}$	b_2	$a_{1,str}$	π_u	σ_g	σ_u
				Sb_3 System				
CCSD(T)/LanL2+dfspd	163	218	114	155	224	35	165	281
CCSD(T)/SBKJ+dfspd	166	224	125		233	36	170	292
B3LYP/LanL2+dfspd	154	215	115	161	228	44	169	282
B3LYP/SBKJ+dfspd	159	222	118	165	234	45	175	291
	(0.1)		(0.1)	(23.5)	(0.1)	(0.2)		(47.2)
				Bi_3 Systems				
CCSD(T)/RECP								
CCSD(T)/LanL2+dfspd	111	150	80		153	80	111	193
CCSD(T)/SBKJ+dfspd	111	151	79	84	153	21	111	180
B3LYP/LanL2+dfspd	110	155	83	114	164	29	119	195
B3LYP/SBKJ+dfspd	110	155	83	113	163	29	118	192
	(0.3)		(0.1)	(15.0)	(0.1)	(0.2)		(29.3)

[a] All symbols have the same meaning as in Table 3.

basis. The all-electron-basis limits are located between the limits for the CCSD(T) and B3LYP limits with the RECP.

The adiabatic energy difference between the $^3B_2$ state of As_3^- and the $^2B_1$ state of As_3 (ΔE in Table 5) is calculated to be 1.71 eV by the CCSD(T)/6-311++G(3df) method. The CCSD(T)/LanL2(SBKJ)+dfspd method underestimates the value by 0.15 eV. On the other hand, the B3LYP/6-311++G(3df) method gives a value of 1.81 eV for ΔE, which is 0.1 eV larger than the value by the CCSD(T)/6-311++G(3df) method. As shown in the discussion of the photoelectron spectrum of P_3^-, the present CCSD(T)/drop-MO calculations tend to underestimate the electron binding energy by about 0.1 eV. As a result, the adiabatic electron binding energy (ABE) calculated using CCSD(T)/6-311++G(3df) must be added by 0.1 eV, whereas the ABE calculated using CCSD(T)/LanL2(SBKJ)+dfspd must be added by 0.2−0.25 eV. We expect that a correction of the same magnitude will need to be made to the vertical electron detachment energy (VBE).

The calculations using the LanL2(SBKJ)+dfspd RECP basis produce vibrational frequencies (ω) very close to the corresponding frequencies calculated using the 6-311++G(3df) basis, as shown in the lower parts of Tables 4 and 6. The calculations using the RECP basis tend to underestimate the harmonic frequencies, although the difference between the values of ω from the 6-311++G(3df) and LanL2(SBKJ)+dfspd bases is usually less than 10 cm^{-1}, with a maximum difference of only 18 cm^{-1} for $\omega(e')$ of the $^4A_1''$ state. We expect a similar reliability in the RECP results for the Sb and Bi trimer systems.

When the values of R_e and $\angle$ calculated using the CCSD(T) and B3LYP methods (shown in Table 5) are compared with the results of Balasubramanian et al.[5] from the MRCI method, the values of $\angle$ are found to be almost the same and the values of R_e are 0.03−0.04 Å shorter in the CCSD(T) and B3LYP results. The excitation energies calculated using the CCSD(T)/RECP method are comparable to those obtained by Balasubramanan et al. No experimental values exist for R_e, $\angle$, and ω of As_3^- and As_3. However, we expect the data in Tables 3−6 to be sufficiently accurate that it can be used to guide future experimental work.

It is now clear that the ground state of As_3^- is the triplet $^3B_2(D_{3h})$ state and not one of the singlet states, $^1A_1(C_{2v})$ and $^1\Sigma_g^+(D_{\infty h})$. This stands in contrast to the assumption of a singlet ground state used previously to analyze the photoelectron spectrum.[10]

3.3. Structure of the Antimony and Bismuth Trimers: Sb_3^-, Sb_3, Bi_3^-, and Bi_3. Only the RECP bases were used in the calculations on the trimer systems of Sb and Bi because of the lack of proper all-electron basis sets and to incorporate relativistic effects. On the basis of the results for the As trimer systems, only the LanL2(SBKJ)+dfspd basis sets were used in the study of the Sb and Bi trimers.

The values of R_e, $\angle$, and ω of Sb_3^- and Bi_3^- are given in Tables 7 and 8. When these values are compared with those in Tables 3 and 4, we find that the value of R_e increases about 0.35 Å on going from As to Sb and about 0.15 Å on going from Sb to Bi. The value of $\angle$ of the $^1A_1$ state of Sb_3^- and Bi_3^- is similar to that of As_3^-. The value of T_e of the $^1A_1$ state with respect to the $^3B_2$ state is almost unchanged on going from As to Sb and Bi, but the value of T_e of the $^1\Sigma_g^+$ state increases from 0.60 eV for As_3^- to 0.90 and 1.03 eV for Sb_3^- and Bi_3^-, respectively.

The potential energy barriers between the $^1A_1$ and $^1\Sigma_g^+$ states in Sb_3^- and Bi_3^- were calculated to be 30.7 and 28.3 kcal/mol, respectively, in the B3LYP/6-31+G(d) calculation. The values

TABLE 9: Results for the Low-lying Doublet and Quartet Electronic States of Sb_3 and Bi_3[a]

	$^2E''(D_{3h})$								$^4E'(D_{3h})$					
	$^2B_1(C_{2v})$			$^2A_2(C_{2v})$			$^4A_1''(D_{3h})$		$^4B_2(C_{2v})$			$^4A_1(C_{2v})$		
	ΔE	R_e	$\angle$	T_e	R_e	$\angle$	T_e	R_e	T_e	R_e	$\angle$	T_e	R_e	$\angle$
						Sb_3 Systems								
CCSD(T)/LanL2+dfspd	1.78	2.841	56.2	+0.05	2.723	64.2	1.36	2.908	1.54	2.765	65.2	1.55	2.891	56.3
CCSD(T)/SBKJ+dfspd	1.80	2.817	56.2	+0.05	2.700	64.2	1.42	2.883	1.59	2.741	65.3	1.61	2.867	56.2
B3LYP/LanL2+dfspd	1.94	2.834	55.8	−0.03	2.720	64.3	1.29	2.909	1.42	2.764	66.0	1.44	2.905	55.8
B3LYP/SBKJ+dfspd	1.96	2.810	55.8	−0.03	2.696	64.3	1.31	2.884	1.48	2.740	66.1	1.50	2.880	55.8
others/MRCI [b]		2.9	55.6	−0.04	2.76	65.8								
						Bi_3 Systems								
CCSD(T)/LanL2+dfspd	1.62	2.984	56.2	+0.05	2.861	64.3	1.14	3.056	1.47	2.915	65.5	1.48	3.060	55.9
CCSD(T)/SBKJ+dfspd	1.63	2.992	56.3	+0.06	2.870	64.3	1.14	3.062	1.48	2.924	65.5	1.48	3.068	55.9
B3LYP/LanL2+dfspd	1.75	2.941	55.8	−0.04	2.825	64.2	1.11	3.012	1.38	2.880	66.1	1.40	3.034	55.5
B3LYP/SBKJ+dfspd	1.78	2.956	55.8	−0.04	2.840	64.2	1.09	3.026	1.37	2.896	66.1	1.39	3.051	55.5
others/MRCI [b]		3.08	55.8	−0.04	2.94	65.6								

[a] All symbols have the same meaning as in Table 5. [b] Reference 5.

TABLE 10: Results for Sb_3 and Bi_3[a]

	$^2E'(D_{3h})$				$^4A_1''(D_{3h})$		$^4E'(D_{3h})$			
	$^2B_1$		$^2A_2$				$^4B_2$		$^4A_1$	
	a_1	a_1	a_1	a_1	a_1'	e'	a_1	a_1	a_1	a_1
					Sb_3 Systems					
CCSD(T)/LanL2+dfspd	234	171	229	149	199	147	214	124	219	158
CCSD(T)/SBKJ+dfspd	240	177	240	155	204	150	219	126	224	162
B3LYP/LanL2+dfspd	241	173	229	151	197	145	209	117	216	153
B3LYP/SBKJ+dfspd	234	162	236	154	202	148	214	120	221	157
	(1.0)	(0.2)	(0.1)	(0.1)		(0.5)	(0.1)	(0.2)	(0.2)	(1.1)
					Bi_3 Systems					
CCSD(T)/LanL2+dfspd	163	124	161	106	137	102	148	87	150	108
CCSD(T)/SBKJ+dfspd	163	120	169	93	137	101	149	86	150	110
B3LYP/LanL2+dfspd	174	124	165	109	144	105	150	85	156	109
B3LYP/SBKJ+dfspd	173	124	164	108	144	105	150	85	155	109
	(0.1)	(0.0)	(0.1)	(0.0)	144	(0.5)	(0.0)	(0.1)	(0.2)	(0.3)

[a] All symbols have the same meaning as in Table 4.

of R_e and $\angle$ of the transition structures are 2.648 Å and 111.6° in Sb_3^- and 2.787 Å and 114.2° in Bi_3^-. The vibrational frequencies decrease on going from As to Sb and decrease a little further on going from Sb to Bi. The bending frequencies of the linear structure of the $^1\Sigma_g^+$ state of Sb_3^- and Bi_3^- are exceptionally small, with values of only ~40 cm^{-1} for Sb_3^- and ~30 cm^{-1} for Bi_3^-.

The results for the low-lying electronic states of Sb_3 and Bi_3, listed in Table 9, show almost the same trends as the results for As_3 shown in Table 5. The degenerate ground $X^2E(D_{3h})$ state splits into $^2B_1(C_{2v})$ and $^2A_2(C_{2v})$ states because of the Jahn−Teller effect. The angles of the two states are almost the same, regardless of the element. The relative energy between the two states is also almost the same; the CCSD(T)/RECP method locates the $^2B_1$ state 0.05−0.06 eV below the $^2A_2$ state, whereas the B3LYP/RECP method predicts the reverse order with an energy gap of 0.03−0.04 eV. Similar relationships are found in the results for the Jahn−Teller pair ($^4B_2$ and $^4A_1$) of the $^4E'(D_{3h})$ state. The bond lengths of the states calculated in the present study are about 0.1 Å shorter than those obtained by Balasubramanian et al.[5]

The magnitude of the Jahn−Teller splittings in the $^2E''$ and $^4E'$ states is calculated to be 0.06 eV. The Jahn−Teller splitting in the $^2E'$ state, however, is 0.3 eV even without including the effect of spin−orbit coupling. The $^2E'$ state of As_3 and Sb_3 also shows a similar magnitude of the Jahn−Teller splitting.

One noticeable difference between the properties of As_3 and those of Sb_3 and Bi_3 concerns the energy gap between the $^4A_1''$ and $^4E'$ states. The two states are almost degenerate in As_3, but the energy gap becomes 0.17−0.19 and 0.28−0.34 eV in Sb_3 and Bi_3, respectively. The value of T_e of the $^4A_1''$ state also changes from ~1.8 eV in As_3 to ~1.3 in Sb_3 and down to ~1.1 eV in Bi_3.

The vibrational frequencies of Sb_3 and Bi_3 are given in Table 10. The frequency of every vibrational mode decreases on going from As to Sb and decreases further on going to Bi. The magnitude of the decrease is larger for stretching modes than for bending modes. Despite these decreases, the relative magnitudes of the frequencies among the different modes of the different states remain the same, regardless of the element. The only discrepancy is that for Sb_3 and Bi_3 the $\omega(a_1')$ of $^4A_1''$ is smaller than the $\omega_{str}(a_1)$ of both $^4B_2$ and $^4A_1$, whereas for As_3 the $\omega(a_1')$ mode lies between the $\omega_{str}(a_1)$ of $^4B_2$ and $^4A_1$.

3.4. Photoelectron Spectroscopy of As_3^-, Sb_3^-, and Bi_3^-. The results of the present calculations were drawn together, and the photoelectron spectroscopy of As_3^-, Sb_3^-, and Bi_3^- was analyzed. The results of this process are presented in Table 11, and the relationship among the electronic states is schematically depicted in Figures 1 and 2.

The CCSD(T) method with open-shell UHF molecular orbitals[39] was used to calculate the vertical electron detachment energies (VBEs) from the triplet state of the anion, $^3B_2$. On the other hand, to prevent the HF convergence problem, the CCSD(T) method with the QRHF molecular orbitals[40] was used for the VBEs from the $^1A_1$ state.

The order of the highest occupied molecular orbitals of the $^1A_1$ state is $\sim b_2^2\, a_1^2\, a_2^2$, the same as shown in Figure 1. The one-

TABLE 11: Adiabatic and Vertical Electron Binding Energies (ABE and VBE in eV) of $M_3^- \xrightarrow{h\nu} M_3$ for M = As, Sb, and Bi

initial state of M_3^-		$^1A_1$					$^3B_2$;$M_3^-(^3A_2')$				$^1\Sigma_g^+$	
final state |of M_3		$^2A_2$		$^4B_2$	$^2A_1$	$^2B_2$	$^2B_1$, $^2A_2$	$^4A_2''$	$^4B_2$, $^4A_1$	$^2B_2$, $^2A_1$	$^2\Pi_g$	$^4\Sigma_g^-$
	δE^a	ABE	VBE	VBE	VBE	VBE	VBE	VBE	(VBE)[g]	VBE	VBE	VBE
						As_3 Systems						
6-311++G(3df)	+0.10	1.49	1.61	3.41	3.49	4.54	1.93, 1.98	3.85	3.84	4.72, 4.95	2.76	4.72
LanL2+dfspd	+0.25	1.46	1.64	3.47	3.52	4.62	1.94, 1.98	3.88	3.89	4.79, 4.79	2.82	4.43
SBKJ+dfspd	+0.25	1.46	1.64	3.99	3.51	4.62	1.94, 1.99	3.87	3.89	4.77, 5.02	2.78	4.51
+MRCI[b]							1.94, 1.99	3.83	4.13	4.67		
expt[c]		~1.45	1.62				1.98					
						Sb_3 Systems						
LanL2+dfspd	+0.20	1.59	1.71	3.19	3.41	4.12	2.06, 2.12	3.43	3.61	4.33, 4.56	2.73	3.83
SBKJ+dfspd	+0.20	1.61	1.72	3.23	3.56	4.18	2.09, 2.15	3.53	3.69	4.42, 4.66	2.77	3.92
+MRCI[b]	+0.20						2.09, 2.13	3.40	3.85	4.30		
expt[d]		~1.85	1.904	3.312			2.061					
expt[e]		1.76	1.91				2.05	3.65				
						Bi_3 Systems						
LanL2+dfspd	+0.20	1.46	1.57	2.95	3.19	3.88	1.90, 1.96	3.04	3.39	4.02, 4.31	2.51	3.07
SBKJ+dfspd	+0.20	1.47	1.58	2.99	3.19	3.89	1.91, 1.97	3.04	3.40	4.02, 4.32	2.50	3.05
+MRCI[b]	+0.20						1.91, 1.95	2.78	3.52	3.88		
expt[e]		1.48	1.61	2.72	3.13	3.76	1.86	2.86	3.31	4.34		
expt[f]		1.48	1.626	2.679			1.895	2.830				~3.1

[a] The ABE and VBE are obtained by adding this correction to actually computed values. [b] The excitation energy of the ref 5 is added to our VBE of the $^2B_1$ state. [c] Reference 10. [d] Reference 7. [e] Reference 9. [f] Reference 6. [g] The average values of the two VBE are given. The differences between two VBEs are less than 0.01 eV here.

electron detachment processes from the $^1A_1$ of M_3^- generate the $^2A_2$, $^2A_1$, and $^2B_2$ states of neutral M_3. Because the a_2(HOMO) and b_1(LUMO) of the $^1A_1$ state stem from the e'' MO by the Jahn−Teller effect, a Penning ionization process can produce a quartet state, $^4B_2$, in which an electron is ejected from the a_1(HOMO-1) while another electron is excited from the a_2(HOMO) to the b_1(LUMO).

As mentioned in previous sections and as shown in our previous work on the photoelectron spectroscopy of Al_3^- [32] and Ag_3^-,[33] the CCSD(T)/all-electron/drop-MO method employed in the present work tends to underestimate the BE by about 0.1 eV. In addition, the CCSD(T)/RECP method underestimates the BE by about 0.15 eV in comparison to the CCSD(T)/all-electron method. To account for these underestimations, the calculated electron-binding energies of As_3^- in Table 11 were obtained by adjusting the values calculated using the CCSD(T)/LanL2(SBKJ)+dfspd and CCSD(T)/6-311++G(3df) methods by +0.25 and +0.10 eV, respectively.

Balasubramanian et al. calculated the T_e of the $^4E'$ and $^2E'$ states of As_3, Sb_3, and Bi_3 using the MRCI method.[5] We added the vertical electron detachment energy (VBE) for the $^2B_1(M_3) \leftarrow {}^3B_2(M_3^-)$ process obtained in the present calculations to the T_e values reported by Balasubramanian et al.; the resulting VBEs of $^4E'$ and $^2E'$ are presented in Table 11 under the label +MRCI.

The photoelectron spectrum of As trimer[10] was reported more recently than the spectra of other elements of group V[6−9] and has received the least analysis and discussion. Only two main peaks, separated by 0.36 eV, are observed in the photoelectron spectrum of As_3^-.[10]

The difference between the ABEs of the two Jahn−Teller components of $^2E''$ ($^2B_1$ and $^2A_2$) is less than 0.05 eV. The difference between the VBE of the two components is also less than 0.05 eV. The magnitudes of the spin−orbit splitting in the ^2D and ^2P states of arsenic atom are only 0.040 and 0.057 eV,[41] respectively. Thus, the spin−orbit coupling effect and the Jahn−Teller effect both seem to be insufficient to account for the splitting of 0.36 eV.

On the other hand, the VBE of the $^2A_2(As_3) \leftarrow {}^1A_1(As_3^-)$ transition is calculated to be 1.64 eV, which is very close to the first peak maximum at 1.62 ± 0.03 eV in the photoelectron spectrum of As_3^-.[10] The ABE of this transition is calculated to be 1.46−1.49 eV, which is also close to the experimentally estimated value of 1.45 ± 0.03 eV. In addition, the VBE of the $As_3(^2B_1$ or $^2A_2) \leftarrow As_3^-(^3B_2)$ transition, calculated to be 1.94−1.98 eV, matches very well with the second peak maximum at 1.98 eV.[10]

The lack of experimental information on the vibrational frequencies of As trimers prevents us from making a more detailed comparison between the results of the present work and experiment. However, our results strongly indicate that the two peaks in the photoelectron spectrum are due to transitions from the $^1A_1$ and $^3B_2$ states.

In Table 11, we also report the VBE of several other electron detachment processes of As_3^-, but at present, no corresponding experimental values exist. The meaning of these additional processes is given below in the discussion of the Sb_3^- and Bi_3^- systems, where some of these processes are observed. We expect that these additional VBE values for As_3^- systems will prove useful in future experimental studies. For completeness, the first two VBEs from the $^1\Sigma_g^+$ state are included in Table 11, although it is not clear if the electron detachment processes from the $^1\Sigma_g^+$ can play any role in the photoelectron spectroscopy of As_3^-.

The photoelectron spectrum of Sb_3^- can be analyzed in a similar way to that of As_3^-. The difference between the two VBEs of the $Sb_3(^2B_1$ and $^2A_2) \leftarrow Sb_3^-(^3B_2)$ transition is only 0.06 eV, almost the same magnitude as in the case of As_3^-. It is clear that the Jahn−Teller effect plays only a minor role in the splitting between the first two peaks in the spectrum of Sb_3^-. Our calculation does not explicitly include the spin−orbit coupling effect, but this effect cannot be ignored in the case of Sb given that the magnitudes of the spin−orbit splitting in the ^2D and ^2P states of antimony atom are 0.166 and 0.257 eV,[41] respectively.

On the basis of the results of the analysis of the photoelectron spectra of P_3^- and As_3^-, the ABE and VBE values of the electron detachment processes from Sb_3^- systems were obtained

by adding 0.20 eV to the computed values. As a result, the VBE of the $^2B_1(Sb_3) \leftarrow {}^3B_2(Sb_3^-)$ transition is 2.06−2.15 eV, which is very close to the experimental values for the second peak of 2.061 and 2.05 eV obtained by Polak et al.[7] and Gausa et al.,[9] respectively.

Even after the correction of +0.20 eV, however, the VBE of the $^2A_2(Sb_3) \leftarrow {}^1A_1(Sb_3^-)$ transition is 1.71 eV, which is 0.2 eV smaller than the experimental values for the first peak of 1.904 and 1.91 eV obtained by Polak et al.[7] and Gausa et al.,[9] respectively. A more rigorous examination of the discrepancy between the theoretical results presented here and experiment would require further calculations that explicitly include the spin−orbit effect.

Polak et al. observed a weak peak corresponding to 3.312 eV BE, and assigned it to the $^4A_2''(D_{3h}) \leftarrow {}^3B_2\ (D_{3h})$ transition.[7] Gausa et al., on the other hand, observed a third peak at 3.65 eV BE with very strong intensity.[9] Our calculated values for VBE suggest that the weak peak at 3.312 eV corresponds to the Penning ionization of $^4B_2(Sb_3) \leftarrow {}^1A_1(Sb_3^-)$, whereas the strong peak at 3.65 eV corresponds to a one electron detachment process, $^4A_2''$ (or the $^4B_2$ and $^4A_1$ of $^4E'$) $\leftarrow {}^3B_2\ (Sb_3^-)$.

Gausa et al. observed eight peaks in the photoelectron spectrum of Bi_3^-,[9] distributed as four pairs of two peaks. Polak et al.[6] also reported the first four of these peaks. The electron binding energies in the two experimental results are within ±0.04 eV. The ABE and VBE values of the Bi trimer systems were calculated using the CCSD(T)/LanL2(SBKJ)+dfspd method, and the resulting values were corrected by +0.20 eV as for the Sb trimers.

The magnitudes of the spin−orbit splitting in the ^2D and ^2P states of bismuth atom are 0.498 and 1.426 eV,[41] respectively. Balasubramanian et al.[5] estimated the magnitude of the spin-orit splitting in the doublet and quartet states of neutral bismuth trimer to be approximately 0.2−0.3 eV. Although it is clear that the spin−orbit effect should play an important role here, the spin−orbit coupling between the singlet and triplet states of the anionic trimer system is not provided anywhere. Because of the lack of the information and on the basis of our analyses of the photoelectron spectra of P_3^-, As_3^-, and Sb_3^-, the photoelectron spectrum of Bi_3^- is tentatively analyzed based only on the fact that Bi_3^- has two low-lying electronic states, $^3B_2$ and $^1A_1$, which are of comparable geometry and energy.

In the lower part of Table 11, the peak maximum of the first peak of each of the four pairs of peaks is compared to the calculated (and corrected) VBE of the transition from the $^1A_1$ state, whereas the peak maximum of the second peak of each pair is compared to the VBE of the transition from the $^3B_2$ state. The agreement between our theoretical VBE values and the experimental peak maxima[6,9] is reasonable but not perfect.

Polak et al. pointed out a broad feature corresponding to a BE of 2.9−3.2 eV.[6] They considered the transition from the $^1\Sigma_g^+$ state to the $^4\Sigma_g^-$ state of Bi_3, which can be connected to a quartet state in the bent structure. According to our calculations, the VBE of the $^4\Sigma_g^- \leftarrow {}^1\Sigma_g^+$ transition is 3.05−3.07 eV, which is very close to the location of the broad feature at 2.9−3.2 eV BE.

As shown by Balasubramanian et al., the $^2\Pi_g$ state does not correspond to a local minimum on the potential energy surface, and converts to either the $^2B_1$ or $^2A_2$ state. The $^2\Pi_g$ state splits into $3/2_g$ and $1/2_g$ states because of the spin−orbit coupling. We calculated the VBE of the transition from $^1\Sigma_g^+$ to $^2\Pi_g$, although it remains unclear as to whether the spin−orbit coupling produces a potential energy barrier in the conversion to the $^2B_1$ and $^2A_2$ states.

4. Conclusions

In section 3.1, all of the features of the photoelectron spectrum of P_3^- are explained by reference to our theoretical results. It was clearly shown that the third peak of the spectrum corresponds to the electron detachment process $P_3(^2\Pi_g) \leftarrow P_3^-(^1\Sigma_g^+)$, and other major peaks correspond to electron detachment processes from the $^3B_2(^3A_2'')$ and $^1A_1(C_{2v})$ states of P_3^- to the $^2B_1$, $^2A_2$, $^4A_2$, $^4A_1$, and $^4B_2$ states of P_3.

In sections 3.2 and 3.3, highly reliable information about the bond lengths, angles, and vibrational frequencies of the low-lying electronic states of the anionic ($^3B_2$, $^1\Sigma_g^+$, and $^1A_1$) and neutral ($^2B_1$, $^2A_2$, $^4A_2$, $^4A_1$, and $^4B_2$) trimer systems of arsenic (As), antimony (Sb), and bismuth (Bi) are provided. Bond lengths increase about 0.35 Å on going from As to Sb and a further 0.15 Å on going from Sb to Bi. The bond angles are very similar regardless of the elements. The vibrational frequencies of the structures are very small (80−350 cm^{-1}). We expect that the information provided here on the geometry and vibrational frequencies of the low-lying electronic states will prove useful in future experimental studies.

In section 3.4, the peaks in the photoelectron spectra of As_3^-, Sb_3^-, and Bi_3^- are analyzed by reference to our theoretical results. One of the most interesting features of the experimental photoelectron spectra of group V elements is the appearance of pairs of peaks with splittings of 0.1−0.3 eV. This observation can be accounted for by the present calculations, which show that the $^3B_2$ and $^1A_1$ states of the anionic trimer have similar energy and geometry. The role of spin−orbit coupling in the trimer systems studied here is not yet clear, because spin−orbit coupling was not explicitly included in the calculations. This omission is potentially important for the Sb and Bi trimers. However, the results of the present work show that the Jahn−Teller effect is less than 0.06 eV, except for the case of the $^2E'$ state where the effect on the VBE is about 0.2−0.3 eV.

The present study provides the most plausible explanation for the main features of the spectra of group V trimers yet to be given; however, the present theoretical values are not completely consistent with the experimental values for Sb and Bi trimers. The most likely source of the imperfect agreement is the omission of the relativistic spin−orbit coupling effect. Therefore, further theoretical work is needed that includeds the spin−orbit coupling effect on the electronic state of not only neutral but also anionic trimer systems.

Our theoretical results also demonstrate that the current experimental information is far from sufficient. To gain a complete understanding of the electronic structures of the trimer systems of group V elements, experiments are needed to probe for several additional peaks in the photoelectron spectra of As_3^- and Sb_3^-.

Acknowledgment. This work is supported by the Korea Research Foundation under Grant No. KRF-99-041-D00232 D3001. Authors thank the helps and comments from Professor Rodney J. Bartlett and Professor Suehiro Iwata.

References and Notes

(1) Archibald, A. W.; Sabin, J. R. *J. Chem. Phys.* **1971**, *55*, 1821.
(2) Murrell, J. N.; Novaro, O.; Castillo, S. *Chem. Phys. Lett.* **1982**, *90*, 421.
(3) Burdett, J. K.; Marsden, C. J. *New J. Chem.* **1988**, *12*, 797.
(4) Hamilton, T. P.; Schaefer, H. F., III. *Chem. Phys. Lett.* **1990**, *166*, 303.
(5) Balasubramanian, K.; Sumathi, K.; Dai, D. *J. Chem. Phys.* **1991**, *95*, 3494.
(6) Polak, M. L.; Ho, J.; Gerber, G.; Lineberger, W. C. *J. Chem. Phys.* **1991**, *95*, 3053.

(7) Polak, M. L.; Gerber, G.; Ho, J.; Lineberger, W. C. *J. Chem. Phys.* **1992**, *97*, 8990.
(8) Jones, R. O.; Gantefor, G.; Hunsicker, S.; Pieperhoff, P. *J. Chem. Phys*. **1995**, *103*, 9549.
(9) Gausa, M.; Kaschner, R.; Seifert, G.; Faehrmann, J. H.; Lutz, H. O.; Meiwes-Broer, K.-H. *J. Chem. Phys*. **1996**, *104*, 9719.
(10) Lippa, T. P.; Xu, S.-J.; Lyapustina, S. A.; Nilles, J. M.; Bowen, K. H. *J. Chem. Phys.* **1998**, *109*, 10727.
(11) Igel-Mann, G.; Stoll, H.; Preuss, H. *Mol. Phys.* **1993**, *80*, 325.
(12) Ballone, P.; Jones, R. O. *J. Chem. Phys.* **1994**, *100*, 4941.
(13) Kaschner, R.; Saalmann, U.; Seifert, G.; Gausa, M. *Int. J. Quantum. Chem.* **1995**, *56*, 771.
(14) Sundararajan, V.; Kumar, V. *J. Chem. Phys.* **1995**, *102*, 9631.
(15) Hamilton, T. P.; Schaefer, H. F., III. *Angew. Chem., Int. Ed. Engl.* **1989**, *28*, 485.
(16) Andrews, L.; Mielke, Z. *J. Phys. Chem*. **1990**, *94*, 2348.
(17) Raghavachari, K.; Trucks, G. W.; Pople, J. A.; Head-Gordon, M. *Chem. Phys. Lett*. **1989**, *157*, 479.
(18) Bartlett, R. D.; Watts, J. D.; Kucharski, S. A.; Noga, J. *Chem. Phys. Lett.* **1990**, *165*, 51.
(19) Advanced Concepts in Electronic Structure Theory (ACES−II). A product of the University of Florida, Quantum Theory Project, developed by J. F. Stanton et al. Integral packages included are VMOL (J. Almlof and P. R. Taylor); VPROPS (P. Taylor); ABACUS (T. Helgaker, H. J. Ha Jensen, P. Jorgensen, J.O lsen, P. R. Taylor).
(20) Becke, A. D. *J. Chem. Phys.* **1993**, *98*, 5648.
(21) Lee, C.; Yang, W.; Parr, R. G. *Phys. Rev. B*, **1988**, *37*, 785.
(22) Frisch, M. J.; Trucks, G. W.; Schlegel, H. B.; Scuseria, G. E.; Robb, M. A.; Cheeseman, J. R.; Zakrzewski, V. G.; Montgomery, J. A., Jr.; Stratmann, R. E.; Burant, J. C.; Dapprich, S.; Millam, J. M.; Daniels, A. D.; Kudin, K. N.; Strain, M. C.; Farkas, O.; Tomasi, J.; Barone, V.; Cossi, M.; Cammi, R.; Mennucci, B.; Pomelli, C.; Adamo, C.; Clifford, S.; Ochterski, J.; Petersson, G. A.; Ayala, P. Y.; Cui, Q.; Morokuma, K.; Malick, D. K.; Rabuck, A. D.; Raghavachari, K.; Foresman, J. B.; Cioslowski, J.; Ortiz, J. V.; Stefanov, B. B.; Liu, G.; Liashenko, A.; Piskorz, P.; Komaromi, I.; Gomperts, R.; Martin, R. L.; Fox, D. J.; Keith, T.; Al-Laham, M. A.; Peng, C. Y.; Nanayakkara, A.; Gonzalez, C.; Challacombe, M.; Gill, P. M. W.; Johnson, B. G.; Chen, W.; Wong, M. W.; Andres, J. L.; Head-Gordon, M.; Replogle, E. S.; Pople, J. A. *Gaussian 98*, revision A.1; Gaussian, Inc.: Pittsburgh, PA, 1998.
(23) (a) Curtiss, L. A.; Jones, C.; Trucks, G. W.; Raghavachari, K.; Pople, J. A. *J. Chem. Phys.* **1990**, *93*, 2537. (b) Curtiss, L. A.; Raghavachari, K.; Trucks, G. W.; Pople, J. A. *J. Chem. Phys*. **1991**, *94*, 7221.
(24) Dunning, T. H., Jr. *J. Chem. Phys*. **1989**, *90*, 1007. Kendall, R. A.; Dunning, T. H., Jr.; Harrison, R. J. *J. Chem. Phys*. **1992**, *96*, 6796.
(25) Francl, M. M.; Pietro, W. J.; Hehre, W. J.; Binkley, J. S.; Gordon, M. S.; DeFrees, D. J.; Pople, J. A. *J. Chem. Phys*. **1982**, *77*, 3654.
(26) McLean, A. D.; Chandler, G. S.; *J. Chem. Phys*. **1982**, *72*, 5639. Clark, T.; Chandrasekhar, J.; Schleyer, P. V. R. *J. Comput. Chem*. **1983**, *4*, 294.
(27) Schafer, A.; Horn, H.; Ahlrichs, R. *J. Chem. Phys*. **1992**, *97*, 2571.
(28) Binning, R. C.; Curtiss, L. A. *J. Comput. Chem*. **1990**, *11*, 1206.
(29) Watts, J. D.; Gauss, J.; Bartlett, R. J. *J. Chem. Phys*. **1993**, *98*, 8718.
(30) Baeck, K. K.; Watts, J. D.; Bartlett, R. J. *J. Chem. Phys.* **1997**, *107*, 3853.
(31) Baeck, K. K, *J. Chem. Phys*. **2000**, *112*, 1.
(32) Baeck, K. K.; Bartlett, R. J. *J. Chem. Phys*. **1998**, *109*, 1334.
(33) Yoon, J.; Kim, K. S.; Baeck, K. K. *J. Chem. Phys*. **2000**, *112*, 9335.
(34) Hay, P. J.; Wadt, W. R. *J. Chem. Phys.* **1985**, *82*, 270; 284; 299.
(35) Stevens, W. J.; Krauss, M.; Basch, H.; Jasien, P. G. *Can. J. Chem*. **1992**, *70*, 612.
(36) González, A. I.; Mó, O.; Yáñez, M. *J. Chem. Phys*. **2000**, *112*, 225.
(37) Scuseria, G. E.; Scahefer, H. F. *Chem. Phys. Lett*. **1988**, *152*, 382.
(38) Watts, J. D.; Bartlett, R. J. *Int. J. Quantum Chem. Symp*. **1993**, *27*, 51.
(39) Watts, J. D.; Gauss, J.; Bartlett, R. J. *J. Chem. Phys*. **1993**, *98*, 8718.
(40) Rittby, M.; Bartlett, R. J. *J. Phys. Chem.* **1988**, *92*, 3033.
(41) Wiese, W. L.; Smith, M. W.; Miles, B. M. *Atomic Transition Probabilities*, National Stand. Ref. Data Ser.; National Bureau of Standards: Washington, D. C., 1969; Vols. I−IV.